Langmuir

ARTICLE

pubs.acs.org/Langmuir

Fibronectin and Bone Morphogenetic Protein-2-Decorated Poly(OEGMA-*r*-HEMA) Brushes Promote Osseointegration of Titanium Surfaces

Xiaoshuai Ren,[†,⊥] Yuanzi Wu,[‡,⊥] Yan Cheng,[†] Hongwei Ma,[*,∥] and Shicheng Wei[*,†,§]

[†]Center for Biomedical Materials and Tissue Engineering, Academy for Advanced Interdisciplinary Studies, [‡]Academy for Advanced Interdisciplinary Studies, and [§]Department of Oral and Maxillofacial Surgery, School and Hospital of Stomatology, Peking University, 100871 Beijing, PR China

[∥]Suzhou Institute of Nano-Tech and Nano-Bionics, Chinese Academy of Sciences, 215123 Suzhou, PR China

Supporting Information

ABSTRACT: To be better used as medical implants in orthopedic and dental clinical applications, titanium and titanium-based alloys need to be capable of inducing osteogenesis. Here we describe a method that allows the facile decoration of titanium surfaces to impart an osteogenesis capacity. A Ti surface was first deposited on a poly(OEGMA-*r*-HEMA) film using surface-initiated atom-transfer radical polymerization (SI-ATRP) with the further step of carboxylation. The modified surfaces were resistant to cell adhesion. Fibronectin (FN) and recombinant human bone morphogenetic protein-2 (rhBMP-2) were further immobilized onto p(OEGMA-*r*-HEMA) matrices. Our results demonstrate that the FN- and rhBMP-2-conjugated polymer surfaces could induce the adhesion of MC3T3 cells on Ti surfaces. Moreover, the protein-tethered surface exhibited enhanced cell differentiation in terms of alkaline phosphatase activity compared to that of the pristine Ti surface at similar cell proliferation rates. This research establishes a simple modification method of Ti surfaces via Ti-thiolate self-assembled monolayers (SAMs) and SI-ATRP and identifies a dual-functional Ti surface that combines antifouling and osseointegration promotion.

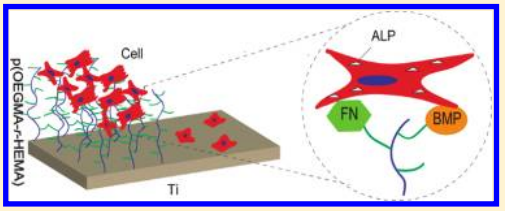

INTRODUCTION

Titanium and titanium-based alloys possess excellent properties (load-bearing, low density, and biocompatibility) and have been widely used as artificial implants in dental, bone replacement, and orthopedic surgery.[1,2] However, Ti-based surfaces suffer from severe limitations: the surfaces are prone to protein adsorption and cell adhesion, a lack of osseointegration, a long healing time, and a risk of infection.

Many efforts have been devoted to Ti surface modification to accelerate bone fixation and the apposition period[3] and reduce infection rates.[4] Such goals could be partially reached by roughening the surface via sand blasting,[5] which induces cell adhesion and the bond between implants and bone tissue. Further treatments such as anodic oxidation,[6] chemical deposition,[7] and biomimetic coating[8] have been explored to improve the bioactivity of titanium. Another concern in concert with promoting osteoblast adhesion is to prevent biofouling, which interferes with the implants' functions. This could be overcome by introducing ethylene glycol chains to prevent nonspecific protein adsorption.[9,10]

However, essential improvements to strengthening the bond of implants and bone tissue might be achieved by introducing bioactive molecules into the tissue−implant interface to promote osseointegration and accelerate the bone-healing process. Although the simple adsorption of protein onto the surface is insufficient to retain the stability and bioactivity in the complicated internal environment,[11] some methods have been developed to covalently immobilize proteins, enzymes, or peptides onto metallic surfaces by means of low-temperature plasma,[11] coupling agents,[12] and surface-initiated polymerization (SIP).[13] Compared with other grafting methods, SIP allows a controlled brush density and thickness[14] as well as the facile tethering of antibioctics, proteins, and peptides.[15,16]

Some peptides and proteins, including collagen,[15] fibronectin (FN),[17] and bone morphogenetic proteins (BMPs),[18] are used to improve the bioactivity of materials. Collagen and FN, parts of ECM proteins, have been proven to promote cell adhesion to substrates.[15,17] BMPs are reported to be able to modulate subsequent cell differentiation and activity at the biomaterial−tissue interface[11,19] and promote osseointegration.[20] Coimmobilizing these two kinds of proteins will have dual functions of promoting cell adhesion as well as cell proliferation and differentiation.[19] The combination of recombinant human bone morphogenetic protein-2 (rhBMP-2) and collagen has been applied in the segmental osseous defects for bone regeneration in prior decades.[21] Also, Giamblanco et al.[22] have confirmed a better performance of cell attachment when FN is coadsorbed with other proteins.

In this article, we develop a method to modify Ti surfaces with sparse polymer brushes of poly(oligo(ethylene glycol) methacrylate)

Received: June 28, 2011
Revised: August 19, 2011
Published: September 02, 2011

Scheme 1. Biofunctionalization of the Ti Surface[a]

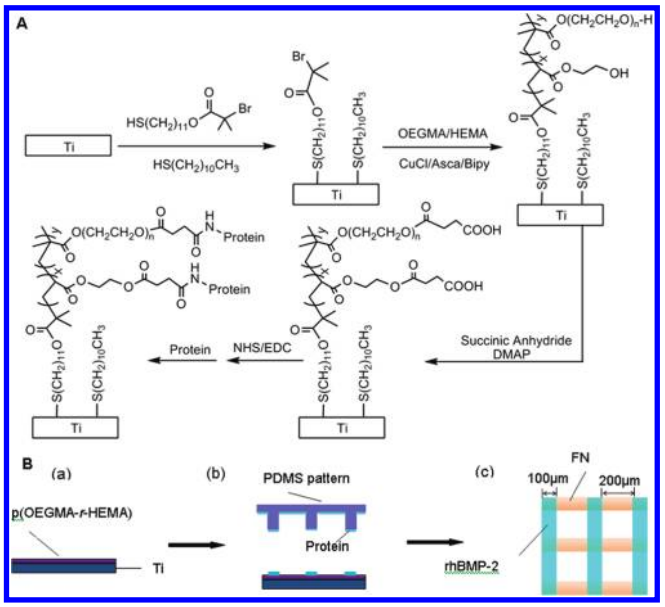

[a] (A) A protein-decorated Ti surface was prepared in four steps, and the formation of an initiator SAM and SIP as well as carboxylation led to a carboxylated poly(OEGMA-*r*-HEMA) coating, to which proteins were immobilized. (B) Protein patterns on Ti with an ~20 nm carboxylated poly(OEGMA-*r*-HEMA) coating were prepared in two steps: the microcontact printing of fibronectin (horizontal) and then rhBMP-2 (vertical), which was then used for cell culturing.

that can resist nonspecific protein adsorption and cell attachment. The side ethylene glycol group was further converted to carboxyl for protein tethering. FN and rhBMP-2 were covalently immobilized onto the polymerized surface. The coated surfaces were subjected to a restricted cell adhesion assay in vitro to give an intuitive view of the antifouling property as well as a cell-adhesion-promoting comparison between FN and rhBMP-2. Furthermore, the cell proliferation and differentiation properties of the bioactive surfaces were evaluated via mouse preosteoblast cell MC3T3-E1 culturing.

EXPERIMENTAL SECTION

The thiolate initiator (ω-mercaptoundecyl bromoisobutyrate) was purchased from HRBio (Suzhou, China). 1-Undecanethiol, oligo(ethylene glycol) methacrylate (OEGMA, M_n = 526), 2-hydroxyethyl methacrylate (HEMA), anhydrous *N*,*N*′-dimethylformamide (DMF), succinic anhydride, and 4-(dimethylamino) pyridine (DMAP) were purchased from Aldrich. *N*-Ethyl-*N*′-(3-dimethylaminopropy)carbodiimide hydrochloride (EDC) and hydroxy-2,5-dioxopyrolidine-3-sulfonic acid sodium (NHS) salt were purchased from Medpep (Shanghai, China). 2-(*N*-Morpho)ethanesulfonic acid was purchased from Merck. FN and rhBMP-2 were purchased from Sigma.

Immobilization of Proteins. Titanium metal (80 nm) was deposited onto a silicon wafer using a magnetron sputtering system (KYKY Technology Development LTD, China). Titanium-coated samples were cleaned with ethanol and distilled water before use. SI-ATRP with poly(OEGMA-*r*-HEMA) was carried out as previously described (Scheme 1A).[17,23] Briefly, mixed SAMs of ω-mercaptoundecyl bromoisobutyrate (initiator) and 1-undecanethiol (spacer) were prepared by immersing the titanium wafer into a 1 mM mixed solution (total concentration) of two thiols with a ratio of 1:2 overnight at room temperature.[23] The surfaces modified with mixed SAMs were thoroughly rinsed with ethanol three times to remove the physisorbed molecules and then dried in a stream of nitrogen. The poly(OEGMA-*r*-HEMA) reaction solution was prepared by mixing well with Milli-Q-water (3 mL), methanol (12 mL), bipyridine (12.5 mg), and monomers OEGMA526 (2.65 g, 5 mM) and HEMA (0.65 g, 5 mM). Another 1 mL of $CuCl_2$ solution (0.04 mM) was added to the mixed solution. After the mixed solution was deoxygenated for 15 min, 1 mL of predeoxygenate-dascorbic acid solution (AscA, 0.04 mM) was injected with a syringe. The mixture was further deoxygenated for another 15 min, and the resulting mixture was transparent red in color. This mixture was then transferred to the reaction setup, and the wafers were immersed in an inert gas glovebox at room temperature. The polymerization was stopped after 6 h, and the wafers were thoroughly rinsed with ethanol and Milli-Q water and dried in a stream of nitrogen. Then the surfaces were incubated in a DMF solution containing succinic anhydride (10 mg/mL) and DMAP (15 mg/mL) for 12 h of carboxylation. FN and rhBMP-2 were tethered to polymer brushes using NHS/EDC chemistry. After being thoroughly washed, samples were incubated in 2.0 mM EDC and 5.0 mM NHS in 0.1 M 2-(*N*-morpho)ethanesulfonic acid for 30 min. For the cell proliferation and differentiation test, FN solution (50 μg/mL in PBS) and rhBMP-2 solution (2.5 μg/mL in PBS) were then incubated on the activated surfaces for 1 h before sterilization. For micropatterning experiments, PDMS stamps with parallel lanes (100 μm in width and 200 μm in line spacing, Scheme 1B(c)) were first inked with FN solution (50 μg/mL) or rhBMP-2 (2.5 μg/mL) solution, respectively, and (EDC/NHS)-activated substrates were then stamped in certain direction for 1 min and exposed to dry air for 30 min for thorough fixation. The treated samples were finally washed with PBS three times and stored in PBS overnight to facilitate protein rearrangement on the polymer matrices for better performance. For immediate use, the surface should be deactivated in ethanol amine (1 M, pH 8.5) for 10 min.

Surface Characterization. Polymer brushes were characterized by goniometry and X-ray photoelectron spectroscopy (XPS). Static water contact angles (CA) were measured by a Dataphysics OCA20 contact angle system (Filderstadt, Germany) at room temperature. Six samples in each stage were used to provide an average and standard deviation of the water contact angle on the material surfaces. XPS was carried out using monochromatic Al Ka X-rays (1486.7 eV) in an AXIS Ultra instrument (Kratos Analytical, Manchester, U.K.). The X-ray source had a 2 mm nominal X-ray spot size operating at 15 kV and 10 mA for both survey and high-resolution spectra. Survey spectra (0−1100 eV) were recorded at a 160 eV pass energy with an energy step of 1.0 eV and a dwell time of 200 ms. High-resolution spectra were recorded at a 40 eV pass energy with an energy step of 0.1 eV and a dwell time of 500 ms with a typical average of three scans. All peaks were referenced to C 1s (CH_x) at 285 eV in the survey scan spectra and C 1s (CH_x) at 284.8 eV in the high-resolution C 1s spectra. All data were collected and analyzed using software provided by the manufacturer.

Osteoblast Cell Culture. Mouse preosteoblast cells (MC3T3-E1, ATCC CRL-2593, USA) were used to investigate the cell behavior on the pristine Ti surface, the FN-immobilized surface, the rhBMP-2-immobilized surface, and both the FN- and rhBMP-2-coimmobilized surfaces (1:1 v/v FN/BMP). MC3T3-E1 cells were cultured in α-modified Eagle's medium (αMEM; Invitrogen, USA) supplemented with 10% (v/v) fetal bovine serum (FBS, Hyclone, USA), 100 U/mL penicillin, and 100 U/mL streptomycin at 37 °C in a humidified 5% (v/v) CO_2 incubator (MCO-18AIC, Japan). When the cells reached 80% confluence, they were trypsinized with 0.25% (w/v) trypsin (Invitrogen Co., USA) and counted with a cytometer (Marienfeld, Germany) prior to being used in the experiments. MC3T3 cells were seeded onto each sample, and assessments of their adhesion, morphology, proliferation, and alkaline phosphatase (ALP) activity at different time points were made.

Assessment of Cell Adhesion and Morphology. To test the cell adhesion and observe the morphology, micropatterning experiments using PDMS stamp as a soft lithography model were applied. We conceived a facile matrix method to test the antifouling property as well as the cell-adhesion-promoting comparison between FN and rhBMP-2. FN (50 μg/mL in phosphate-buffered saline) and rhBMP-2 (2.5 μg/mL in phosphate-buffered saline) were stamped onto the same (EDC/NHS)-activated sample in a perpendicular direction for 1 min, hence the two proteins form a "#" on the polymer-grafted surfaces (Scheme 1B(c)). Cells were seeded on the sterilized substrates at 1×10^5 cells/mL. The surfaces after 24 h of incubation were washed three times with PBS to remove the loosely adsorbed cells. Cells were fixed with 2.5% glutaraldehyde for 1 h, followed by dehydration with gradient ethanol solutions for 15 min. A metallographic microscope (Olympus BX51M, Japan) was used to image the patterned surface with immobilized cells.

Assessment of Cell Proliferation. The MC3T3-E1 cell proliferation on different modified surfaces was assessed at days 1, 4, and 7. Each sample was cut into a square shape with dimensions of around 8×8 mm^2 and placed into 24-well plates. Cells were seeded on the sterilized substrates at 4×10^4 cells/mL. The culture medium was renewed every 3 days during the whole cell culturing period. At the end of each time point, the absorbance was determined by a 3-(4,5-dimethylthiazol-2-yl)-2,5-diphenyltetrazolium bromide (MTT) assay (Sigma, USA). Briefly, 40 μL of the MTT reagent was added to the 400 μL culture medium of each well, and after 4 h of incubation, 400 μL of the formazan solubilization solution (10% SDS in 0.01 M HCl) was added to each well and incubated overnight. The absorbance of the samples was measured by a microplate reader (Bio-Rad 680, USA) at a wavelength of 570 nm with a reference wavelength of 630 nm. Six samples were measured for each group at different time points.

Assessment of Cell Differentiation. The sample for the assessment of cell differentiation was prepared as described in the section on cell proliferation. ALP assays were also assessed at days 1, 4, and 7. Briefly, after the culture medium was aspirated, 400 μL of the ALP substrate solution containing 10 mM pNPP (Sigma, USA) and 2 mM $MgCl_2$ in a carbonate buffer solution was added to each well. After reaction for 30 min at 37 °C, 100 μL of 1 M NaOH was added to end the reaction. The absorbance was measured with a microplate reader (Bio-Rad 680, USA) at a wavelength of 405 nm. Six samples were measured in each group at different time points.

Statistical Analysis. The data are presented as the mean ± standard deviation ($n = 6$ if not mentioned). Statistical analysis was performed using SPSS 17.0, and P values of <0.05 using a one-way analysis of variance (ANOVA) test were considered to be a statistically significant difference.

RESULTS AND DISCUSSION

Surface Modification and Characterization. The initiators were immobilized onto a Ti surface via self-assembly technology.[24] Compared to other self-assembled monolayers (SAMs) such as silanes and phosphonic acid,[25] thiolate-based SAM were used less in Ti modification because a thick layer of native TiO_2 hinders the formation of a dense SAM. However, our previous work showed that a sparse polymer coating from a low-density initiator SAM via SIP was better at immobilizing large biomolecules such as protein.[26] Furthermore, it is easier to control the quality and density of Ti-thiolate-based SAMs. The latter can be easily realized by altering the ratio of initiator and undecanethiol. Poly(OEGMA-*r*-HEMA) brushes were prepared via 6 h of SIP, which led to a thickness of 20 nm that was specifically chosen for a well-balanced antifouling property and protein immobilization capacity.[26] The polymer-coated surfaces were characterized by goniometry (Table 1) and X-ray photoelectron spectroscopy. The presence of a polymer coating was first identified by a water contact angle test. The pristine Ti substrates were hydrophobic with a contact angle of ~99°, which decreased to an average value of 54° after polymerization. This could be explained by the hydrophilicity of the grafted polymer brush with an OEG side chain. This conclusion was further ascertained by an XPS survey (Figure 1 and Table 2). The pristine Ti surface showed strong Ti 2p and O 1s peaks as well as C 1s resulting from a contaminated hydrocarbon. After SIP from the Ti surface, the Ti 2p signal decreased from 18.0 to 8.1% and the O 1s signal decreased from 50.7 to 42.7%. A substantial increase in the C signal was detected from 31.3 to 49.2%, which indicated the existing of a polymer layer. After carboxylation, the Ti signal decreased to 2.1% and the C signal remarkably increased to 64.6% as a result of the addition of butyrate groups. Moreover, XPS allowed us to distinguish between different element species in different chemical environments in core-level separating spectra: the core spectra of C 1s (Figure S1A) clarify the three typical separating peak components corresponding to C−H/C−C (~285 eV), C−O (~286.5 eV), and C═O groups (~289 eV) in poly(OEGMA-*r*-HEMA),[14,27] indicating the presence of PEG-terminated polymer brushes. The O 1s core spectra (Figure S1B) show a distinctive chemical shift of the broad peak (~532.5 eV) attributed to the complicated polymer from the pristine Ti−O groups (~530 eV). The polymer signal attributed to O 1s (~532.5 eV) was ~7.9 times

Table 1. Water Contact Angles of Ti Surfaces in Different Phases of rhBMP-2 Immobilization

	pristine Ti	polymer-grafted Ti	(EDC/NHS)-activated Ti	rhBMP-2-immobilized Ti
contact angle (mean ± SD)[a]	98.7 ± 1.1°	54.4 ± 2.0°	20.7 ± 1.7°	13.7 ± 2.2°

[a] $n = 6$.

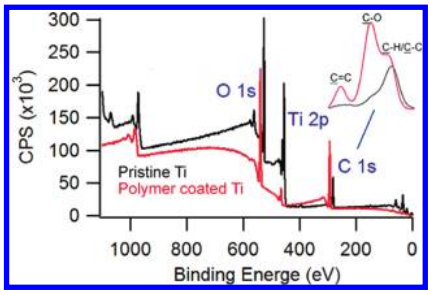

Figure 1. XPS survey scan spectra of pristine Ti (black) and polymer-grafted Ti after carboxylation (red). Enlarged core scan spectra of C 1s (inset). The x axis of pristine Ti (black) was shifted right by 20 eV to give a distinct comparison. See the text and Table 2 for a detailed discussion.

Table 2. Elemental Composition of Pristine Ti and Polymer-Grafted Ti as Determined by XPS

atom ratio (%)	pristine Ti	Ti-p(OEGMA-*r*-HEMA)	Ti-p(OEGMA-*r*-HEMA)-COOH
O 1s	50.7	42.7	33.3
C 1s	31.3	49.2	64.6
Ti 2p	18.0	8.1	2.1

the TiO_2 signal attributed O 1s (~530 eV) after carboxylation, which was ~0.11 times before polymerization, indicating the presence of the polymer covering up the Ti surface. Further evidence of carboxylation of the terminal hydroxyl was confirmed by the difference in the oxygen component ratio (O 1s (~532.5 eV)/O 1s (~530 eV)) before and after carboxylation, which indicated the addition of butyrate groups to the side chain of the polymer brush. From the data above, we conclude the successful coating of p(OEGMA-*r*-HEMA)-COOH on the Ti surface.

Osteoblast Attachment to Ti-p(OEGMA-*r*-HEMA) Surfaces. To immobilize protein on the Ti surface presenting polymer brushes, the hydroxyl end groups of poly(OEGMA-*r*-HEMA) were further converted to carboxyl via succinic anhydride coupling, which is reactive to the amine groups of proteins (Scheme 1A). The −COOH groups on the resulting Ti-p(OEGMA-*r*-HEMA)-COOH surfaces were preactivated with EDC/NHS chemistry to facilitate the protein tethering of terminal carboxyl groups to NHS groups, producing protein tethering surfaces.[26] To promote cell adhesion and induce bone formation on the Ti surface, rhBMP-2 was immobilized on Ti surfaces.[28] The contact angle showed a decrease from 20.7 to 13.7° after rhBMP-2 tethering, which indicated the success of the immobilization process.

Our previous work showed background levels of protein adsorption (~0.5 ng/cm^{-2}) on P(OEGMA-*r*-HEMA)-COOH surfaces, as measured by surface plasmon resonance (SPR).[26] To demonstrate further the antifouling property of P(OEGMA-*r*-HEMA)-COOH on Ti surfaces, MC3T3 cells were cultured on pristine Ti (Figure S2a) and polymer-coated surfaces (Figure S2b). The polymer-brush-coated Ti surfaces were resistant to cell adhesion. In contrast to the antifouling surface, cells adhered to and spread well on the pristine Ti surface. Furthermore, a poly(dimethylsiloxane) (PDMS) stamp with micrometer-scale lanes was first inked with FN, a model bioadhesive ligand enhancing the cell−biomaterial integration,[9,17] and rhBMP-2. Then the stamp was microcontact printed (μCP) onto the Ti surfaces presenting activated polymer matrices. To make an intuitive comparison, a combinatorial printing method for multiplexed proteins was utilized (Scheme 1B): first one PDMS stamp was inked with FN and placed in contact with the Ti substrate, and the protein was printed in a horizontal orientation. In the second stage, another PDMS stamp was inked with rhBMP-2 placed in contact with and printed on the same Ti substrate in a vertical orientation, finally resulting in the cross reticular architecture of proteins. One day after seeding, the "bare" Ti-P(OEGMA-*r*-HEMA)-COOH surface showed few cell adhesions, indicating that the antifouling surfaces resisted mammalian cell adhesion and activation. FN lanes adhered to the patterned district and constrained most of the MC3T3 cells, but fewer cells were retentively adhered to the rhBMP-2-tethered strips (Figure 2). This can be explained by the fact that BMPs can stimulate the adhesion and proliferation of osteoblastic cells;[29] however, as a signaling protein that delivers extracellular signals to the nucleus, rhBMP-2 plays a subordinate role in cell adhesion and spreading, compared with FN.

Osteoblast Proliferation and Differentiation Evaluation. Further quantitative examinations of long-term cell performance on different Ti surfaces were conducted for 1 week. The cell proliferation of MC3T3 cell assays was performed via an MTT assay on pristine Ti, with FN immobilized, rhBMP-2 immobilized, and FN + BMP coimmobilized. On day 1, the rhBMP-2-immobilized surface supported the lowest levels of cell adhesion, which could be explained by the resulting compromise of the cell-resistant form of the PEG-based substrate and the tethering of proteins for cell adhesion promotion. On days 4 and day 7, the cells showed similar proliferation rates on all of the surfaces (Figure 3), and the phenomenon was consistent with the results previously reported by other groups who immobilized collagen,[30] fibronectin,[31] and rhBMP-2[32] on biomaterials, respectively.

To investigate the differentiation of osteoblasts and check the osteogenesis of different Ti surfaces, the ALP activity was also tested with MC3T3-E1 mouse preosteoblast cells. In accordance with the cell proliferation, the ALP activities on all surfaces increased as time went on. On days 1 and 4, no significance in different groups was observed. However, the rhBMP-2-modified surfaces had much higher ALP activities compared with the

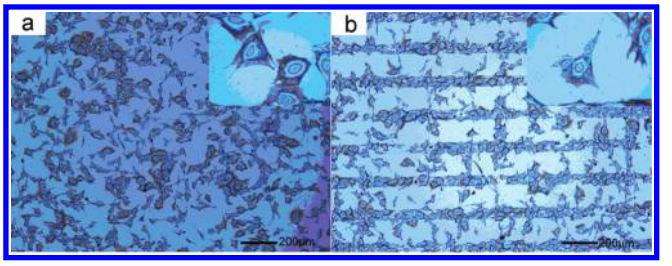

Figure 2. Microscopy images of MC3T3 cells on (a) pristine Ti and (b) an FN-patterned surface (horizontal) and an rhBMP-2-patterned Ti surface (vertical) after 24 h of MC3T3 seeding (10^5 cells/mL). The inset is the enlargement of the single cell.

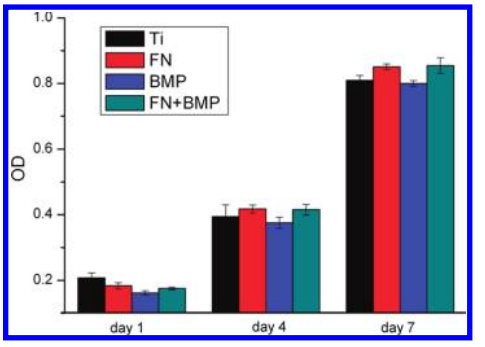

Figure 3. Proliferation differences in MC3T3 cells on four surfaces, namely, pristine Ti-, FN-, BMP-, and (FN + BMP)-coated Ti surfaces. The number of cells per well was measured with a 3-(4,5-dimethylthiazol-2-yl)-2,5-diphenyltetrazolium bromide (MTT) assay and expressed as the optical density (OD).

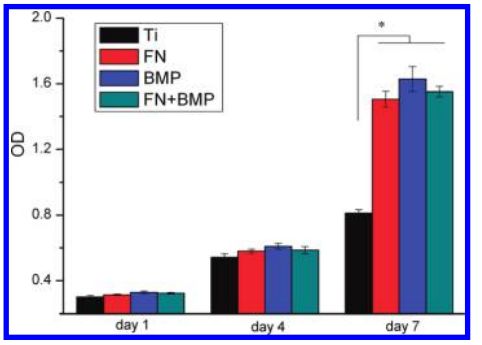

Figure 4. ALP activity of MC3T3 cells on four surfaces after 1, 4, and 7 days. * denotes significant differences ($P < 0.05$) between the marked groups using ANOVA.

pristine Ti surfaces on day 7, which confirmed the high level of ALP in the cells and indicated the differentiation of MC3T3-E1 into osteoblasts (Figure 4). It should be pointed out that the ALP activity was higher on the modified surfaces only in the later period of the test cycle (day 7), which may be due to the slow release rate of proteins caused by the covalent immobilization procedure. It is an unexpected result that FN-tethered Ti surfaces showed a similar level of ALP activity as compared to that of BMP- or (BMP + FN)-tethered Ti surfaces. Several possible explanations may be attributed to this result: As an important ECM-protein-mediating cell surface and other ECM components, FN participates in the biological activities in terms of enhancing the cellular differentiation.[33,34] It is also conceivable that the higher FN concentration (50 μg/mL for FN vs 2.5 μg/mL for rhBMP-2) may influence the ALP activity comparison. However, more studies are needed to explain the mechanism of the two proteins' induced cell proliferation and differentiation.

CONCLUSIONS

We developed a dual-functional titanium surface with antifouling- and osseointegration-promoting properties via a facile, versatile strategy: immobilization of the initiator on the Ti surface followed by the surface-initiated polymerization of poly(OEGMA-*r*-HEMA) and the tethering of FN and rhBMP-2. The low-density ethylene glycol-terminated polymer brushes are effective at resisting protein nonspecific adsorption and cell adhesion. After further functionalization to display bioactive ligands, the osteogenetic titanium surface for osteoblastic cell adhesion was achieved uniformly or constrained to micropatterned domains. The protein-tethered surface showed comparable cell adhesion and proliferation to those of pristine Ti surfaces with improved cell differentiation in terms of the alkaline phosphatase activity. We believe that the facile method offers a promising strategy for the fabrication of titanium-based biomedical devices with both the antifouling nature and immobilization of osteogenetic and bioadhesive ligands.

ASSOCIATED CONTENT

Supporting Information. C 1s and O 1s core scan spectra of pristine Ti and Ti-p(OEGMA-r-HEMA) before and after carboxylation as determined by XPS. Elemental composition of Ti-p(OEGMA-r-HEMA) before and after carboxylation as determined by XPS. Microscopy images of MC3T3 cells on pristine Ti- and p(OEGMA-r-HEMA)-COOH-coated Ti surfaces without NHS/EDC activation. This material is available free of charge via the Internet at http://pubs.acs.org.

AUTHOR INFORMATION

Corresponding Author

*(H.M.) E-mail: hwma2008@sinano.ac.cn. Tel/Fax: 86512-62872-539. (S.W.) E-mail: sc-wei@pku.edu.cn. Tel/Fax: 8610-82195780.

Author Contributions

⊥These two authors contributed equally to this article.

ACKNOWLEDGMENT

This work was supported by the NSFC (21074148), the State Key Development Program for Basic Research of China (2007CB936103), and the Fundamental Research Funds for the Central Universities.

REFERENCES

(1) Geetha, M.; Singh, A. K.; Asokamani, R.; Gogia, A. K. *Prog. Mater. Sci.* **2009**, *54*, 397–425.
(2) Vannoort, R. *J. Mater. Sci.* **1987**, *22*, 3801–3811.
(3) Lin, A.; Wang, C. J.; Kelly, J.; Gubbi, P.; Nishimura, I. *Int. J. Oral Maxillofac. Implants* **2009**, *24*, 808–816.
(4) Hu, X. F.; Neoh, K. G.; Shi, Z. L.; Kang, E. T.; Poh, C.; Wang, W. *Biomaterials* **2010**, *31*, 8854–8863.
(5) Ruger, M.; Gensior, T. J.; Herren, C.; von Walter, M.; Ocklenburg, C.; Marx, R.; Erli, H. J. *Acta Biomater.* **2010**, *6*, 2852–2861.
(6) Galli, C.; Coen, M. C.; Hauert, R.; Katanaev, V. L.; Groning, P.; Schlapbach, L. *Colloids Surf., B* **2002**, *26*, 255–267.
(7) Rohanizadeh, R.; LeGeros, R. Z.; Harsono, M.; Bendavid, A. *J. Biomed. Mater. Res., Part A* **2005**, *72A*, 428–438.
(8) Lin, D. Y.; Wang, X. X. *Colloids Surf., B* **2011**, *82*, 637–640.
(9) Capadona, J. R.; Collard, D. M.; Garcia, A. J. *Langmuir* **2003**, *19*, 1847–1852.
(10) Petrie, T. A.; Capadona, J. R.; Reyes, C. D.; Garcia, A. J. *Biomaterials* **2006**, *27*, 5459–5470.
(11) Puleo, D. A.; Kissling, R. A.; Sheu, M. S. *Biomaterials* **2002**, *23*, 2079–2087.
(12) Balasundaram, G.; Webster, T. J. *J. Biomed. Mater. Res., Part A* **2007**, *80*, 602–611.
(13) Raynor, J. E.; Petrie, T. A.; Garcia, A. J.; Collard, D. M. *Adv. Mater.* **2007**, *19*, 1724–1728.
(14) Fan, X. W.; Lin, L. J.; Messersmith, P. B. *Biomacromolecules* **2006**, *7*, 2443–2448.
(15) Zhang, F.; Shi, Z. L.; Chua, P. H.; Kang, E. T.; Neoh, K. G. *Ind. Eng. Chem. Res.* **2007**, *46*, 9077–9086.
(16) Petrie, T. A.; Stanley, B. T.; Garcia, A. J. *J. Biomed. Mater. Res., Part A* **2009**, *90*, 755–765.
(17) Wu, Y. Z.; Coyer, S. R.; Ma, H. W.; Garcia, A. J. *Acta Biomater.* **2010**, *6*, 2898–2902.
(18) Kang, S. M.; Kong, B.; Oh, E.; Choi, J. S.; Choi, I. S. *Colloids Surf., B* **2010**, *75*, 385–389.
(19) He, X. Z.; Ma, J. Y.; Jabbari, E. *Langmuir* **2008**, *24*, 12508–12516.
(20) Leknes, K. N.; Yang, J.; Qahash, M.; Polimeni, G.; Susin, C.; Wikesjo, U. M. E. *Clin. Oral. Implants Res.* **2008**, *19*, 1027–1033.
(21) Hollinger, J. O.; Schmitt, J. M.; Buck, D. C.; Shannon, R.; Joh, S. P.; Zegzula, H. D.; Wozney, J. *J. Biomed. Mater. Res.* **1998**, *43*, 356–364.
(22) Giamblanco, N.; Yaseen, M.; Zhavnerko, G.; Lu, J. R.; Marletta, G. *Langmuir* **2011**, *27*, 312–319.
(23) Wu, Y. Z.; Huang, Y. Y.; Ma, H. W. *J. Am. Chem. Soc.* **2007**, *129*, 7226–7227.
(24) Akbulut, M.; Alig, A. R. G.; Israelachvili, J. *J. Phys. Chem. B* **2006**, *110*, 22271–22278.
(25) Helmy, R.; Fadeev, A. Y. *Langmuir* **2002**, *18*, 8924–8928.
(26) Ma, H. W.; He, J. A.; Liu, X.; Gan, J. H.; Jin, G.; Zhou, J. H. *ACS Appl. Mater. Interfaces* **2010**, *2*, 3223–3230.
(27) Ma, H. W.; Li, D. J.; Sheng, X.; Zhao, B.; Chilkoti, A. *Langmuir* **2006**, *22*, 3751–3756.
(28) Li, X. L.; Cao, X. BMP Signaling and Skeletogenesis. In *Skeletal Development and Remodeling in Health, Disease, and Aging*; Zaidi, M, Eds.; Blackwell Publishing: Boston, 2006; pp 26−40.
(29) Shah, A. K.; Lazatin, J.; Sinha, R. K.; Lennox, T.; Hickok, N. J.; Tuan, R. S. *Biol. Cell* **1999**, *91*, 131–142.
(30) van den Dolder, J.; Jansen, J. A. *J. Biomed. Mater. Res., Part A* **2007**, *83A*, 712–719.
(31) Salmeron-Sanchez, M.; Rico, P.; Moratal, D.; Lee, T. T.; Schwarzbauer, J. E.; Garcia, A. J. *Biomaterials* **2011**, *32*, 2099–2105.
(32) Shi, Z. L.; Neoh, K. G.; Kang, E. T.; Poh, C. K.; Wang, W. *Biomacromolecules* **2009**, *10*, 1603–1611.
(33) Pankov, R.; Yamada, K. M. *J. Cell Sci.* **2002**, *115*, 3861–3863.
(34) Mao, Y.; Schwarzbauer, J. E. *Matrix Biol.* **2005**, *24*, 389–399.